Linear Results on the Barrier Effects of Mesoscale Mountains

R. T. PIERREHUMBERT

Geophysical Fluid Dynamics Laboratory/NOAA, Princeton University, Princeton, NJ 08542

(Manuscript received 17 August 1983, in final form 3 January 1984)

ABSTRACT

We examine the factors determining whether a mountain acts as a strong barrier to an impinging flow. A primary concern is the extent to which the barrier effect is reduced when smoothed orography is used in a numerical model. These questions are addressed within the model of linear, rotating, stratified flow over topography first studied by Queney. The ground-level Green's functions for this model are derived and their near- and far-field asymptotic behavior is discussed. Using the asymptotic results, the upstream deceleration is estimated as a function of $\mathrm{Ro} = U/fL$ and $\bar{h}_m = Nh_m/U$, where U is the far upstream speed of the cross-mountain flow, f the Coriolis parameter, L the mountain width, N the Brunt-Väisälä frequency, and h_m is the maximum mountain height. Effects of terrain shape are also considered. The Green's functions are evaluated numerically and used to calculate the response to a family of mountain profiles; a comparison with asymptotic results shows the latter to be very useful. It is concluded that preserving maximum terrain height of ridgelike features is superior to preserving an integrated quantity such as mountain volume. Both the Alps and the Rocky Mountains exert a pronounced barrier effect which would not generally be preserved in present numerical models using smoothed orography.

1. Introduction

Representing the effects of the Earth's orography in numerical models is highly problematic. Most of the major mountain ranges, notably the Rockies, Alps, Andes, and Himalayas, vary in height by several kilometers over horizontal scales that cannot be resolved within existing models. This implies that some sort of misrepresentation of terrain shape is inevitable. Given that the terrain must in some way be distorted, it is important to know what terrain characteristics need to be preserved in order to minimize the errors in model response. Commonly, the average terrain height within a grid length is used to generate the model orography. However, there is no logical reason to expect that preservation of the mountain volume (which holds for smoothed orography) should be more important than preservation of some other quantity, such as maximum terrain height (which is reduced in the process of smoothing). The nature of the errors introduced by the smoothing of orography will be a major theme of this paper.

A clear illustration of the above issue may be found in the phenomenon of cyclogenesis in the lee of the Alps. It has long been apparent to researchers attempting to simulate this class of events that the use of smoothed orography drastically reduces the effects of the Alps on cyclogenesis. Bleck (1977), Mesinger and Strickler (1982), and Tibaldi and Buzzi (1982) all had to make use of some form of enhanced orography in order to reproduce cyclogenesis. In all these cases, the orographic enhancement had the effect, broadly speaking, of preserving the height of the barrier to atmospheric flow presented by the Alps. Indeed, Egger (1972) was able to reproduce some features of Alpine cyclogenesis in a low resolution model in which the Alps were represented as a vertical wall. Buzzi and Tibaldi (1978) have noted the importance of mountain-induced distortion of cold fronts in lee cyclogenesis; this feature is probably responsible for the importance of preserving the barrier effect of the Alps.

In order to determine the appropriate height for a mountain range in a numerical model, it is necessary to delineate the circumstances under which a mountain is expected to act like a barrier. This requires an understanding of the nature and magnitude of the forces which cause air to decelerate and turn aside as it approaches a mountain. Likewise, it is necessary to know the effect of terrain shape on the amount of upstream deceleration. In the present work, we will discuss these questions only insofar as they can be addressed within linear theory. While linear theory has obvious shortcomings, it can provide valuable insight as to the appropriate nondimensional parameters and length scales. Moreover, by examining the amplitude of the predicted linear response, we can define the limits of applicability of linear theory; this gives us a means for distinguishing the weak response parameter regime from the strong response regime.

The vehicle for this study will be the model of rotating, stratified flow over a ridge first studied by Queney (1947). The two-dimensional geometry of this model is appropriate for the elongated ridge-like mountains that are of greatest interest in connection

with the blocking of flow. The Queney problem has been extensively studied, and has repeatedly proved a useful tool for the exploration of problems in mountain meteorology. Given the long history of the problem, we wish to emphasize the physical interpretation and implications of the formulas presented in the present work without claiming the discovery of any completely novel phenomena within the model. Nevertheless, through the use of Green's function methods, we believe that we can give a more general and systematic account of the response of the model to arbitrary terrain shapes than has previously appeared.

In the present work we will concentrate on the pattern of deceleration upstream of the mountain, though some downstream features will also be discussed. The discussion will emphasize the pattern of flow near the ground, as this is where the blocking effect is expected to be strongest. We will pay particular attention to the role of the Coriolis force in limiting the magnitude and upstream extent of the strongly decelerated region. Smith (1982) noted that there is a great difference between flow blocking in the quasi-geostrophic and ageostrophic cases. A primary contribution of the present work is to identify the terrain shapes for which strong upstream deceleration is expected to occur. In addition, our approach avoids the difficulties associated with the non-uniform validity of the large Rossby number expansion used by Smith. Results to be presented below also provide some insight as to the spatial domain and range of parameters within which the large Rossby number expansion is useful.

In Section 2 we review the equations defining the Queney model and derive integral expressions for the Green's functions of the horizontal velocity components. In Section 3 the near-field and far-field asymptotic properties of the Green's functions are discussed. Section 4 gives precise numerical evaluations of the Green's functions, and presents a series of velocity patterns for a range of terrain sizes and shapes. We show there that the actual Green's functions can be reconstructed quite well from asymptotic formulas alone. Finally, in Section 5 we summarize and discuss the key results of our study.

We note in passing that Wallace *et al.* (1983) have recently pointed out that the use of smoothed orography can also lead to an underestimation of the forcing of Rossby waves in numerical models. In linear theory, however, the forcing of Rossby waves is truly proportional to the mountain volume (provided the smoothed terrain feature remains small in comparison to the wavelength of the stationary Rossby wave). Therefore, a treatment of the driving of Rossby waves by mesoscale terrain features requires a consideration of nonlinear effects. The linear theory developed in the present work nevertheless contributes indirectly to the resolution of this issue by defining the range in which flow near the mountain is expected to be nonlinear; it is only in this nonlinear range that alternatives to the use of smoothing need be considered.

2. Green's functions for the Queney model

Consider stationary flow on the f-plane over a two-dimensional ridge with height $h(x)$. Let y be the direction parallel to the ridge and z be altitude. Further, let the velocity components in the x-, y-, and z-directions be u, v, and w, respectively. Suppose further that the mountain is low enough that we may linearize about a constant (positive) flow U in the x-direction and a density profile $\rho = \rho_0 + \rho_z z$, where ρ_0 and ρ_z are constants. Finally, assume the flow to be Boussinesq, hydrostatic and incompressible. The resulting system is one of the many models studied by Queney (1947). The equations and some salient features of the solutions are reviewed by Smith (1979, pp. 156–160).

In what follows, we will deal with nondimensional quantities with velocities measured in terms of U, horizontal lengths in terms of $1/k_f$, and vertical lengths in terms of $1/k_s$, where $k_f = f/U$ is the inertial wavenumber and $k_s = N/U$ is the hydrostatic gravity wavenumber. Where necessary, we will use overbars to distinguish nondimensional quantities. We seek Green's functions $\bar{G}_u$ and $\bar{G}_v$ such that the perturbation velocities induced by an arbitrary profile $\bar{h} = Nh/U$ are

$$\frac{u'}{U} = \int_{-\infty}^{\infty} \bar{G}_u(\bar{x} - \bar{x}')\bar{h}(\bar{x}')d\bar{x}', \tag{1}$$

$$\frac{v'}{U} = \int_{-\infty}^{\infty} \bar{G}_v(\bar{x} - \bar{x}')\bar{h}(\bar{x}')d\bar{x}', \tag{2}$$

at $z = 0$. Equation (3.28) of Smith (1979) gives the general expression for the streamline displacement caused by a mountain with Fourier transform $\hat{h}(k)$. The corresponding velocities are easily obtained from the momentum and continuity equations, whence the Green's functions are obtained by taking $\hat{h} = 1/\pi$, corresponding to a δ-function mountain. The results are

$$\bar{G}_u(\bar{\eta}) = \frac{-i}{2\pi}\int_{-\infty}^{\infty} \bar{\gamma}(\bar{k})e^{-i\bar{k}\bar{\eta}}d\bar{k}, \tag{3}$$

$$\bar{G}_v(\bar{\eta}) = -\frac{1}{2\pi}\int_{-\infty}^{\infty} \frac{\bar{\gamma}(\bar{k})}{\bar{k}}\, e^{-i\bar{k}\bar{\eta}}d\bar{k}, \tag{4}$$

where the nondimensional vertical wavenumber $\bar{\gamma}$ is given by

$$\bar{\gamma}(\bar{k}) = \begin{cases} i|\bar{k}|(1 - \bar{k}^2)^{-1/2} & \text{for } |\bar{k}| < 1 \\ -\bar{k}(\bar{k}^2 - 1)^{-1/2} & \text{for } |\bar{k}| > 1. \end{cases} \tag{5}$$

Application of a radiation condition at $z = \infty$ is implicit in (5). In deriving these results, we have effected the incompressibility assumption by taking $s = 0$ in Smith's Eq. (3.28), and the hydrostatic assumption by neglect-

ing k compared to k_s in Smith's Eq. (3.30). Note that the two Green's functions are related by

$$\bar{G}_u = -\partial_{\bar{\eta}}\bar{G}_v. \tag{6}$$

This relation obtains by virtue of the simple form of the y-momentum equation (dimensionally $U\partial_x v' = -fu'$) attained in the two-dimensional limit.

In the following sections, we will discuss the properties of (3) and (4) and their implications. Some consequences of the hydrostatic approximation are mentioned in Section 3b, while compressibility effects are discussed in Section 3c and three-dimensional effects in Section 5.

3. Asymptotic properties of the Green's functions

a. *Far-field asymptotics*

In the following we consider the form of the Green's functions for large positive or negative values of their argument $\bar{\eta}$. When $\bar{\eta}$ is large, the exponential factors in (3) and (4) are rapidly oscillating, and the stationary phase approximation can be used. In this connection, "large $\bar{\eta}$" refers to values of $\bar{\eta}$ much larger than unity, corresponding to dimensional distances much greater than the inertial length $1/k_f = U/f$. Many of the formulas discussed below could have been obtained in terms of results presented by Queney (1947); however, the far-field asymptotic behavior proceeds from an entirely straightforward application of the stationary phase approximation, and so we have chosen to derive the formulas directly from (3) and (4).

Consider first the far-field behavior of $\bar{G}_v(\bar{\eta})$. Applying the stationary phase approximation, we find that there are two stationary phase points which dominate the far-field behavior. The first is near the point $\bar{k} = 0$ and the second is at the singularity of the integrand at the inertial wavenumber $|\bar{k}| = 1$. The latter point corresponds to an integrable square-root singularity at $\bar{k} = \pm 1$. The contribution from this inertial singularity can be made to appear either on the upstream side (negative η) or the downstream side (positive $\bar{\eta}$), depending on the choice of position of the branch cut of the square root appearing in (5). It is easy to show on the basis of group velocity arguments that the train of inertial waves arising from the singularity at $\bar{k} = \pm 1$ should be made to appear on the downstream side. The *far upstream* behavior of $\bar{G}_v$ is then dominated by the contribution from $\bar{k} = 0$.

Evaluating the contribution from $\bar{k} = 0$ by elementary means, we find that the far upstream form of $\bar{G}_v$ is given by

$$\bar{G}_v(\bar{\eta}) = -\frac{1}{\pi\bar{\eta}}, \quad \bar{\eta} \ll -1. \tag{7}$$

This is precisely the Green's function for quasi-geostrophic flow over a mountain. The tendency of the flow to return to geostrophic equilibrium far upstream was first pointed out by Queney (1947). Since $\bar{G}_v$ is positive for negative $\bar{\eta}$, the streamlines deviate to the left as they approach the mountain from the upstream side. The far upstream form of $\bar{G}_u$ is then obtained from (6), resulting in

$$\bar{G}_u(\bar{\eta}) = -\frac{1}{\pi\bar{\eta}^2}. \tag{8}$$

The deviation from U (which is entirely ageostrophic) is negative in the upstream region. Hence the flow decelerates and turns to the left as it approaches the mountain. Note, however, that the deceleration decays quite rapidly with distance upstream of the mountain.

Applying (1) and (2), the far upstream velocities caused by a mountain $\bar{h}(\bar{x})$ are

$$\frac{u'(\bar{x})}{U} = -\frac{1}{\pi}\int_{-\infty}^{\infty} d\bar{x}' \frac{\bar{h}(\bar{x}')}{(\bar{x}-\bar{x}')^2}, \tag{9}$$

$$\frac{v'(\bar{x})}{U} = -\frac{1}{\pi}\int_{-\infty}^{\infty} d\bar{x}' \frac{\bar{h}(\bar{x}')}{(\bar{x}-\bar{x}')}. \tag{10}$$

Consider a localized mountain, so that $\bar{h}(\bar{x})$ vanishes outside of an interval of dimensional length L. The corresponding nondimensional mountain width is $fL/U = 1/\mathrm{Ro}$, where Ro is the Rossby number based on mountain width. Then, for upstream distances with $|x| \gg 1/\mathrm{Ro}$, the integrands in (9) and (10) are nearly constant and the velocity fields become

$$\frac{u'(\bar{x})}{U} = \frac{-1}{\pi\bar{x}^2}\int_0^{1/\mathrm{Ro}} \bar{h}(\bar{x}')d\bar{x}', \tag{11}$$

$$\frac{v'}{U} = \frac{-1}{\pi\bar{x}}\int_0^{1/\mathrm{Ro}} \bar{h}(\bar{x}')d\bar{x}'. \tag{12}$$

Thus, *for upstream distances large compared to the width of the mountain, the velocity field is completely determined by the cross-sectional area of the mountain.* Accordingly, the streamline displacement occurring far upstream is controlled by the cross-sectional area of the mountain, which is proportional to the *average* height. Significant streamline displacements can occur in the far upstream region, because (12) implies that the streamline displacement, which is proportional to the integral of v, diverges logarithmically as $\bar{x} \to -\infty$. The far upstream streamline displacement is limited only by three-dimensional effects.

We now use (9) to derive a general estimate of the deceleration near the mountain in the limit of small Ro. This may be done by progressively broadening the mountain while keeping its shape constant. To this end we write

$$\bar{h}(\bar{x}) = \bar{h}_m F(\mathrm{Ro}\bar{x}), \tag{13}$$

where $\bar{h}_m$ is the mountain height and $F(r)$ is a function vanishing at $r = 0$ and $r = 1$ with maximum value unity. Substituting (13) into (1) and using (8),

$$\frac{u'(0)}{U} = \bar{h}_m \int_0^a \bar{G}_u(-\bar{x}')F(\mathrm{Ro}\bar{x}')d\bar{x}' - \frac{\bar{h}_m}{\pi}\int_a^{1/\mathrm{Ro}} \frac{F(\mathrm{Ro}\bar{x}')}{\bar{x}'^2}\,d\bar{x}', \quad (14)$$

where a is the upstream distance required for the far-field asymptotics to become valid. We will see in Section 4 that $a \approx 1$. As $\mathrm{Ro} \to 0$, the first integral vanishes provided $G_u F$ is integrable, whence

$$\frac{u'(0)}{U} = -\mathrm{Ro}\bar{h}_m \int_{a\mathrm{Ro}}^1 \frac{F(r)}{r^2}\,dr \quad (15)$$

in the limit, in which we have substituted $r = \mathrm{Ro}x$. If $dF/dr = 0$ at $r = 0$, the integral in (15) is O(1) as $\mathrm{Ro} \to 0$; otherwise it has a weak logarithmic divergence and may thus be regarded as O(1) except for exceedingly small values of Ro. Since $\bar{h}_m = Nh_m/U$, where h_m is the dimensional mountain height, $\bar{h}_m$ may be regarded as the internal Froude number. Hence, *for mountains characterized by a small Rossby number, the maximum relative deceleration* u'/U *appearing upstream of the mountain scales with the product of the Rossby number (*Ro = U/fL*) and the Froude number (*$\bar{\mathrm{h}}_\mathrm{m}$ = Nh$_\mathrm{m}$/U*). Significantly,* $\mathrm{Ro}\bar{h}_m = (N/f)(h_m/L)$ is independent of the speed of the flow directed against the mountain. If the mountain slope is greater than f/N, then flow impinging on the mountain will be strongly decelerated even if it is so slow that the Rossby number becomes very small.

We now briefly consider the far downstream form of the Green's functions. Applying the stationary phase approximation to (3) and (4), the dominant contribution is found to arise from the singularities at the inertial wavenumbers $\bar{k} = \pm 1$. For $\bar{\eta} \gg 1$, the Green's functions have the asymptotic form

$$\bar{G}_u(\bar{\eta}) = \left(\frac{2}{\pi}\right)^{1/2} \cos\left(\bar{\eta} - \frac{\pi}{4}\right)(\bar{\eta})^{-1/2}, \quad (16)$$

$$\bar{G}_v(\bar{\eta}) = -\left(\frac{2}{\pi}\right)^{1/2} \sin\left(\bar{\eta} - \frac{\pi}{4}\right)(\bar{\eta})^{-1/2}. \quad (17)$$

The far downstream response consists of a slowly decaying train of inertial waves. Because of their slow downstream decay, the inertial wave train dominates the geostrophic response in the lee, and the ground-level velocities do not relax to geostrophic equilibrium far downstream. At downstream distances much greater than the width of the mountain, the velocity fields obtained from (1) and (2) are

$$\frac{u'}{U} = \left(\frac{2}{\pi\bar{x}}\right)^{1/2}\left[\cos\left(\bar{x} - \frac{\pi}{4}\right)\int_{-\infty}^{\infty} d\bar{x}'\bar{h}(\bar{x}')\cos(\bar{x}') + \sin\left(\bar{x} - \frac{\pi}{4}\right)\int_{-\infty}^{\infty} d\bar{x}'\bar{h}(\bar{x}')\sin(\bar{x}')\right], \quad (18)$$

$$\frac{v'}{U} = -\left(\frac{2}{\pi\bar{x}}\right)^{1/2}\left[\sin\left(\bar{x} - \frac{\pi}{4}\right)\int_{-\infty}^{\infty} d\bar{x}'\bar{h}(\bar{x}')\cos(\bar{x}') - \cos\left(\bar{x} - \frac{\pi}{4}\right)\int_{-\infty}^{\infty} d\bar{x}'\bar{h}(\bar{x}')\sin(\bar{x}')\right]. \quad (19)$$

Hence, *the downstream velocity field is determined neither by the maximum mountain height, nor by its cross-sectional area, but by the projection of the mountain profile on the inertial wave.* Only when the mountain is very narrow compared to the inertial wavelength (i.e., when $\mathrm{Ro} \gg 1$) does this projection become proportional to the cross-sectional area of the mountain.

The far upstream and far downstream asymptotic results discussed above depend only on the longwave contribution to (3) and (4). Therefore, the results are unaffected by the hydrostatic approximation.

b. *Near-field asymptotics*

In the following we will consider the behavior of the Green's functions for $|\bar{\eta}| \ll 1$. This domain is complementary to the far-field domain considered in Section 3a. In this case, it is convenient to find the asymptotic form of $\bar{G}_u$ and then recover $\bar{G}_v$ from (6). We first note that, since $\bar{\gamma}(\bar{k}) = \mathrm{O}(1)$ for large $\bar{k}$, the integral in (3) diverges as $\bar{\eta} \to 0$. Hence, $\bar{G}_u(\bar{\eta})$ is singular at $\bar{\eta} = 0$, and its small $\bar{\eta}$ behavior is determined by the contribution to the integral from large values of $\bar{k}$. Consequently, the asymptotic form of $\bar{G}_u$ at small $\bar{\eta}$ is found by replacing $\bar{\gamma}$ in (3) with its large $\bar{k}$ limit, yielding

$$\bar{G}_u(\bar{\eta}) = \frac{i}{2\pi}\int_{-\infty}^{\infty} s(\bar{k})e^{-i\bar{k}\bar{\eta}}d\bar{\eta} \quad \text{for} \quad |\bar{\eta}| \ll 1, \quad (20)$$

where $s(\bar{k}) = 1$ for positive $\bar{k}$ and $s(\bar{k}) = -1$ for negative $\bar{k}$. Upon carrying out the integral, we find

$$\bar{G}_u(\bar{\eta}) = \frac{1}{\pi}\mathcal{P}\left(\frac{1}{\bar{\eta}}\right) \quad \text{for} \quad |\bar{\eta}| \ll 1, \quad (21)$$

in which $\mathcal{P}(1/\bar{\eta})$ denotes the principal part of $1/\bar{\eta}$. Equation (6) then implies that, to leading order, the near-field form of G_v is

$$\bar{G}_v(\bar{\eta}) = -\frac{1}{\pi}\ln|\bar{\eta}| \quad \text{for} \quad |\bar{\eta}| \ll 1. \quad (22)$$

Equation (21) is identical to the Green's function for waves in a non-rotating, stratified fluid. This is so because the short waves which dominate the near field are unaffected by rotation. In the near field, then, u is determined by the non-rotating problem and v is determined by the small Coriolis force arising from u. The very same result would be obtained from an application of the large Rossby number expansion described by Smith (1982); this confirms that the large Rossby number expansion gives only the near-field behavior of large Rossby number flow. In Section 4

we will show precisely how far from a mountain the near-field behavior remains valid. Upstream of an obstacle, (21) implies that the near field u' is negative and (22) implies that the near field v' is positive, so that flow approaching the mountain slows down and is deflected to the left. The combination of these two effects can lead to a large near-field deflection of flow around an obstacle. The upstream flow is also decelerated in the far field [see (8)], but the far-field deceleration decays much more rapidly with distance from the obstacle than does the near field-deceleration ($1/\bar{\eta}^2$ vs $1/\bar{\eta}$).

Next, we consider the scaling of the deceleration in the large Ro limit. As in Section 3a, we write the mountain profile in the form (13), so that the nondimensional mountain width is 1/Ro. As Ro is made large, the mountain becomes sufficiently small that for the purposes of computing flow near the mountain the entire mountain falls within the scope of the near-field Green's functions. Substituting (21) and (13) into (1) yields

$$\frac{u'(\bar{x})}{U} = \frac{\bar{h}_m}{\pi} \int_{\mathrm{Ro}\bar{x}'=0}^{1} \frac{F(\mathrm{Ro}\bar{x}')}{(\mathrm{Ro}\bar{x}) - (\mathrm{Ro}\bar{x}')}\, d(\mathrm{Ro}\bar{x}'). \quad (23)$$

This formula is valid whenever $|\bar{x}| \ll 1$. From (23) it is obvious that the *maximum deceleration appearing upstream of the obstacle is proportional to the internal Froude number* $\bar{h}_m = Nh_m/U$. In the large Ro limit, then, the upstream deceleration depends only on the maximum mountain height, and is independent of the width of the mountain. The constant of proportionality, of course, depends on the overall shape of the mountain. To address the effect of terrain shape, it is useful to consider a triangular mountain of the form

$$F(r) = \begin{cases} r/r_1 & \text{for} \quad 0 \leqslant r \leqslant r_1 \\ \dfrac{1-r}{1-r_1} & \text{for} \quad r_1 \leqslant r \leqslant 1. \end{cases} \quad (24)$$

For this F, (23) may be integrated analytically; at $x = 0$ (the foot of the mountain) the result is

$$\frac{u'(0)}{U} = \frac{-\bar{h}_m}{\pi} \frac{\ln(1/r_1)}{1-r_1}. \quad (25)$$

An important consequence of this formula is that the deceleration becomes greater as the upwind slope becomes larger ($r_1 \to 0$). In fact, the deceleration becomes infinite as the upwind face becomes vertical, calling to mind the result of Miles and Huppert (1969) on stratified flow over a step. It should also be emphasized that it is only the shape of the mountain that matters. The deceleration given by (25) is insensitive to the mountain width.

Unlike the far-field behavior, the near-field asymptotics are affected by the hydrostatic approximation. This is so because the near field is determined by the short-wave contribution to (3) and (4), and waves with $k > k_s$ are influenced by nonhydrostatic effects. The nonhydrostatic effects on waves with $k > k_s$ will alter the behavior of the Green's functions for small distances $|\eta| < \mathrm{O}(1/k_s)$. There will nevertheless be a considerable range $\mathrm{O}(1/k_f) \gg |\eta| \gg \mathrm{O}(1/k_s)$, within which the near-field form of the hydrostatic Green's function applies.

c. *Depth scales of mountain-induced motions*

As we have discussed only the flow pattern at the ground, it is instructive to estimate the depth scales over which the pattern remains coherent. We obtain this estimate by examining well-known solutions for quasi-geostrophic and for hydrostatic nonrotating flow over a bell-shaped mountain $h = h_m L^2/(x^2 + L^2)$. The former regime will be typical of broad mountains characterized by small Ro, while the latter will be typical of narrow mountains characterized by large Ro.

First, consider the quasi-geostrophic case. Assuming constant N and incompressibility, the along-mountain velocity v is given by Eq. (3.26) of Smith (1979). This formula may be put in the form

$$v = -(Nh_m) \frac{x/L}{(x/L)^2 + [1 + z/(fL/N)]^2}, \quad (26)$$

whence it is clear that the velocity decays monotonically in height with a characteristic depth scale fL/N. From the y-momentum equation u' is easily found to be

$$\frac{u'}{U} = \left(\frac{Nh_m}{fL}\right) \frac{[1 + z/(fL/N)]^2 - (x/L)^2}{\{[1 + z/(fL/N)]^2 + (x/L)^2\}^2}. \quad (27)$$

At the ground, there is deceleration for $|x| > L$. The perturbation reverses sign at $z = (x/L - 1)(fL/N)$ and thereafter decays to zero with characteristic depth fL/N. From this we conclude that, for a mountain characterized by small Ro, the depth of the mountain-induced circulation is on the order of fL/N. With $L = 50$ km, as might be appropriate for the Alps, fL/N is only 500 m for typical N. It is evident that the quasi-geostrophic response to an Alpine-scale mountain would be very shallow.

The solution for the hydrostatic, nonrotating case may be obtained from Eq. (2.55) of Smith (1979) and the continuity equation. In the incompressible limit, u' is given by

$$\frac{u'}{U} = (k_s h_m) \frac{\sin(k_s z) + (x/L)\cos(k_s z)}{1 + (x/L)^2}. \quad (28)$$

The maximum ground-level deceleration occurs at $x = -L$; at this x, the perturbation wind changes sign at $z = \pi/(4k_s)$. Hence, for a mountain characterized by large Ro, the surface deceleration pattern is expected to remain coherent over a depth that is $\mathrm{O}(1/k_s)$. In

contrast to the quasi-geostrophic solution, the winds in the nonrotating case do not decay with height. The infinite influence depth in the nonrotating case would in reality be limited by dissipation, three-dimensionality, and dispersion induced by the Coriolis force. Nevertheless, the possibility exists that the influence of a mountain with large Ro will extend to altitudes considerably above the mountain.

We are now equipped to assess the magnitude of compressibility effects. If H is the density scale-height of the atmosphere and D is a characteristic vertical scale of the mountain-induced motion, then compressibility effects will be small as long as D/H is small. For the small Ro case, this requirement becomes $fL/(NH) \ll 1$, which states that compressibility effects are small when the width of the mountain is small compared to the internal radius of deformation based on the scale height. This requirement is easily satisfied for the Alps, as well as for a number of mountain ranges of the North American cordillera (including the Front Range, the Sierra Nevada and the Brooks Range). In the large Ro case, compressibility is unimportant near the ground as long as $1/(k_s H) \ll 1$, though even if this condition is satisfied, compressibility will have an order-unity effect on the wave amplitude if allowed to act over a sufficient depth. In either case, the possibility must be admitted that even small compressibility effects may have important physical consequences. This is the case for the permanent turning which compressibility introduces, as discussed amply by Smith (1979).

4. Numerical results

In this section, we present a number of numerical calculations illustrating the utility of the asymptotic results discussed above. The asymptotic formulas are summarized in Table 1. Consider first the Green's functions. We calculated G_u and G_v numerically from (3) and (4) using a fast Fourier transform with 2^{14} points and a wavenumber cutoff at $\bar{k} = \pm 40$. The remaining large-$\bar{k}$ contribution was evaluated analytically. The numerical evaluations along with the near- and far-field asymptotic results are displayed in Figs. 1a and b. It is evident that the asymptotic formulas capture all the qualitative features of the Green's functions; moreover, the numerical and asymptotic results are in reasonable quantitative agreement even in the intermediate range $\bar{\eta} = O(1)$. Of particular interest is the value of $\bar{\eta}$ at which the solution begins to resemble the far-field behavior more than the near-field behavior. From Fig. 1 it is found that this occurs between $\bar{\eta} = 0.5$ and 1 (dimensionally, between $0.5k_f^{-1}$ and k_f^{-1}). Hence, one need not go very far from a mountain before the far-field behavior dominates. For $U = 10$ m s^{-1} and $f = 10^{-4}$ s^{-1}, this distance is only 50 to 100 km. In this example, the flow immediately over a 100 km wide mountain would be dominated by the nonrotating near-field solution, but the flow would adjust to geostrophy almost immediately upstream.

TABLE 1. Summary of the asymptotic formulas.

	$\bar{G}_u(\bar{\eta})$	$\bar{G}_v(\bar{\eta})$
Far upstream $\bar{\eta} \ll -1$	$-\frac{1}{\pi}\frac{1}{\bar{\eta}^2}$	$-\frac{1}{\pi}\frac{1}{\bar{\eta}}$
Near field $\lvert\bar{\eta}\rvert \ll 1$	$\frac{1}{\pi}\frac{1}{\bar{\eta}}$	$-\frac{1}{\pi}\ln\lvert\bar{\eta}\rvert$
Far downstream $\bar{\eta} \gg 1$	$\left(\frac{2}{\pi}\right)^{1/2}\cos\left(\bar{\eta}-\frac{\pi}{4}\right)(\bar{\eta})^{-1/2}$	$-\left(\frac{2}{\pi}\right)^{1/2}\sin\left(\bar{\eta}-\frac{\pi}{4}\right)(\bar{\eta})^{-1/2}$

Next, we consider the flow induced by an isosceles triangular mountain with full width L_2 such that $k_f L_2 = 2$. The results were obtained by convolution of the numerically computed Green's functions with the mountain profile. In Fig. 2 we show the results for $\bar{h}_m = k_s h_m = 1$. On the mountain itself, the u' pattern exhibits near-field characteristics, with deceleration appearing on the upwind side and acceleration on the downwind side. The maximum deceleration of $-0.4\bar{h}_m$ is well estimated by the near-field formula (25), which yields $-0.4412\bar{h}_m$ for an isosceles triangle ($r_1 = 0.5$). As predicted by far-field asymptotic theory, the deceleration decays rapidly upstream, falling off by a factor of more than 4 between the foot of the mountain ($k_f x = -1$) and a distance $1/k_f$ upstream ($k_f x = -2$). In the nonrotating case, the u' pattern would be exactly antisymmetric about the mountain crest. The considerable enhancement of the actual downslope acceleration compared to the upslope deceleration reflects the fact that the far-downstream behavior of $\bar{G}_u$ (which begins near $\bar{\eta} = 0.5$) decays much less rapidly with distance than the near-field behavior, as evidenced in Fig. 1a.

The along-mountain wind v' also exhibits predominantly near-field behavior on the mountain; v' is generally positive both upstream and downstream of the crest, as would be expected from the logarithmic near-field behavior of $\bar{G}_v$ shown in Table 1. Also, as expected from the far-upstream asymptotics, v' decays slowly upstream of the mountain, as compared to u'. Downstream of the mountain, both u' and v' are characterized by a pronounced inertial wave. This also is predicted by the asymptotics. As the nondimensional mountain width $k_f L_2$ is rather less than the nondimensional inertial wavelength of 2π, (18) and (19) imply a considerable projection on the inertial wave. We also note that the minimum v' precedes the minimum u', as expected from Fig. 1.

The pattern we have just described is typical of all "mesoscale mountains," that is, mountains with Ro

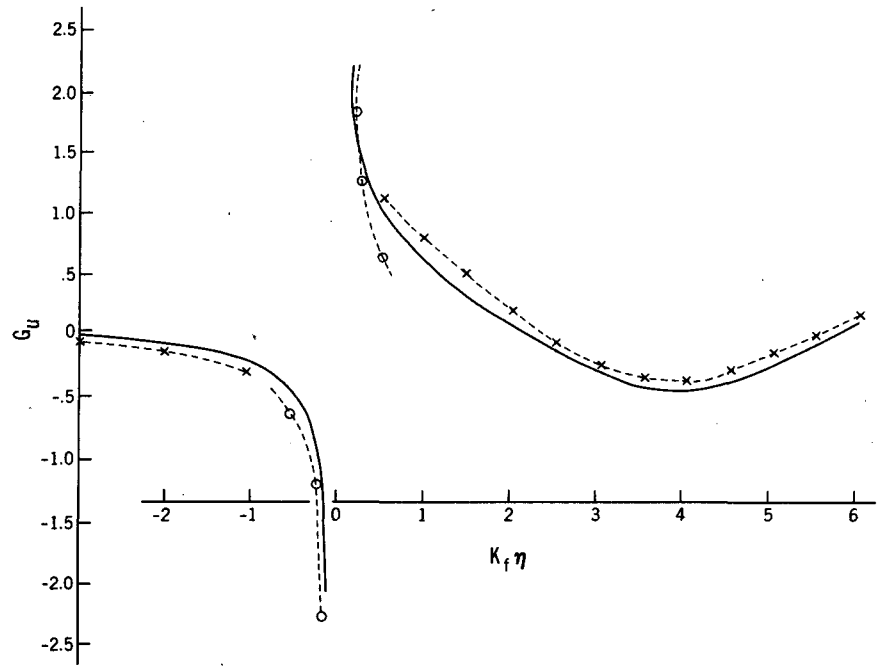

FIG. 1a. Nondimensional Green's function G_u and its approximations. Dashed lines with crosses: far-field approximation. Dashed lines with circles: near-field approximation. Solid lines: numerical evaluation.

of order unity. Fig. 2 corresponds to Ro = $1/(k_f L_2)$ = 0.5. If the mountain is made narrower, Ro increases and a number of changes occur in the pattern. Since the area of the mountain decreases, the strength of the inertial wave decreases. The u' field becomes more symmetric but does not diminish appreciably in amplitude, since the near-field of u' suffers only a rescaling of its argument as Ro is changed [see (23)]. On the other hand, the maximum v' on the mountain decreases, since the logarithmic singularity of G_v is in-

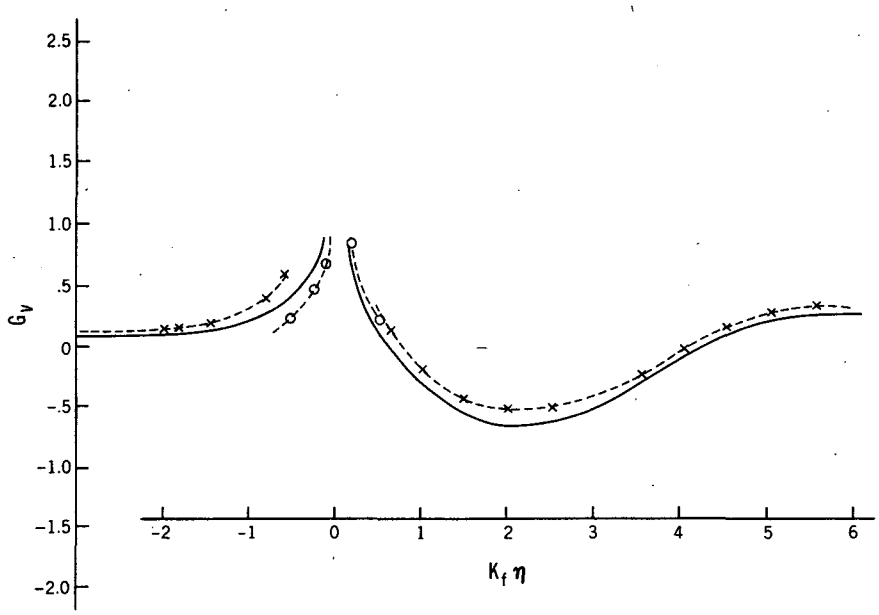

FIG. 1b. Nondimensional Greens function G_v and its approximations. Symbols as for Fig. 1a.

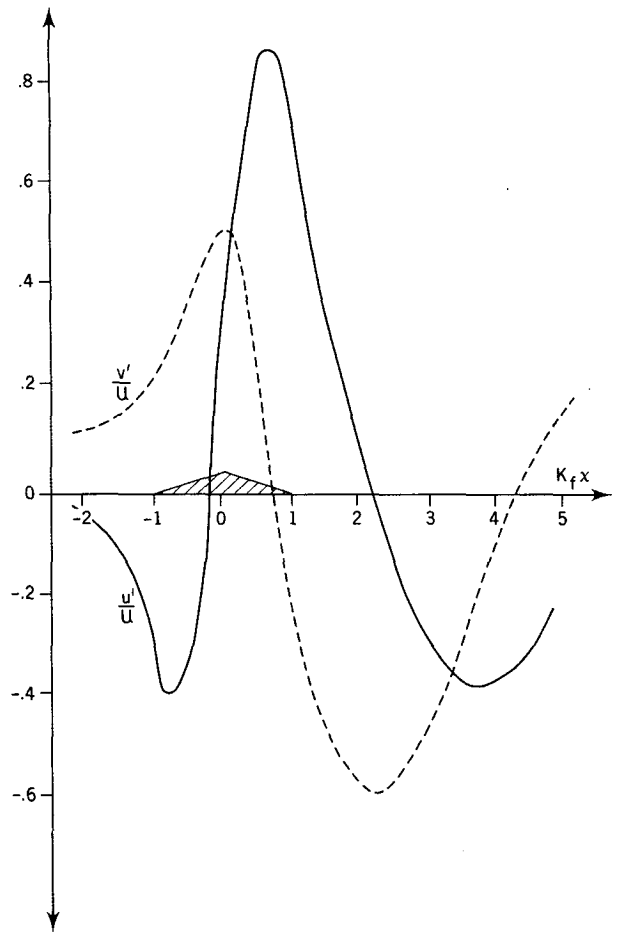

FIG. 2. Cross-mountain wind (u') and along-mountain wind (v') induced by an isosceles triangular mountain of full width $k_fL = 2$ and height $K_sh_m = 1$, where $k_f = f/U$ and $k_s = N/U$.

tegrable. Now consider the effects of decreasing Ro, by increasing k_fL_2. The inertial wave will increase in amplitude until near $k_fL_2 = \pi$. Thereafter it will weaken, owing to destructive interference of waves emitted by different parts of the mountain, as evidenced in (18) and (19). This cancellation does not become very effective until k_fL_2 approaches 2π. The minimum u' on the upwind face diminishes, as more of the mountain comes into the range of the rapidly decaying far-upstream approximation. Because of the presence of the downstream inertial waves, the pattern on the downwind side of the mountain will not closely resemble the customary quasi-geostrophic pattern until values of k_fL_2 rather greater than 2π are reached. The flow on the upwind side, by contrast, will begin to resemble quasi-geostrophic theory at considerably smaller values of k_fL_2 (larger Ro).

In Fig. 3 we show the effects of varying terrain scale and shape. For a family of triangular mountains with full width L_2 and an upstream leg of width L_1, we computed $u'_{\min}/U$, where $u'_{\min}$ is the minimum cross-mountain velocity perturbation appearing upstream of the mountain peak. This quantity gives a simple measure of the extent to which flow is impeded by the mountain. In the results shown, the mountain height was held fixed at $k_sh_m = 1$; as the problem is linear, results for an arbitrary mountain height are obtained by simply multiplying by the appropriate value of k_sh_m. We first note that broadening the mountain with L_1/L_2 fixed decreases the deceleration. This is so because broadening the mountain reduces Ro and, as seen in Section 3a, the deceleration scales with $\mathrm{Ro}\bar{h}_m$ in the small Ro limit. The curves for $k_fL_2 = 1$ and 2 closely follow each other. This is to be expected, as the deceleration is determined primarily by the near field for these values, and therefore is relatively insensitive to the breadth of the mountain. It is only for values of Ro (based on L_2) below 0.5 that the small Ro scaling begins to become effective. We also see that the deceleration increases monotonically as the slope of the upwind face is increased. For $k_fL_2 = 1$ and 2, this is essentially a reprise of the near-field behavior exhibited in (25). In the broad mountain case $k_fL_2 = 5$ we may estimate the upstream deceleration by using the near-field Green's function (21) for distances $|\bar{\eta}| < 1$, and the far-field Green's function (8) for distances $|\bar{\eta}| > 1$. Assuming $k_fL_1 > 1$, the perturbation x-velocity at the upstream foot ($x = 0$) is

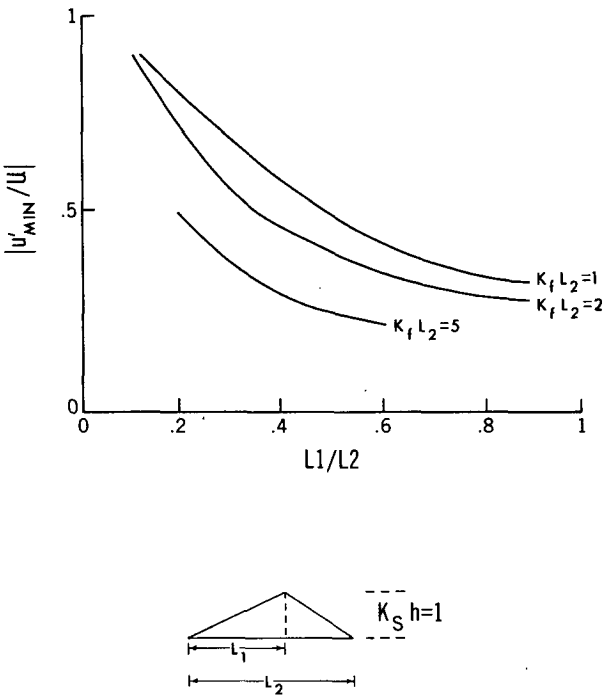

FIG. 3. Maximum deceleration appearing upstream of mountain crest for a family of triangular mountains with full width L_2 and upstream leg of width L_1.

$$\frac{u'(0)}{U} = \frac{-1}{\pi}\frac{N}{f}\frac{h_m}{L_1}\left[1 + \ln(k_f L_1) - \frac{\ln(L_2/L_1)}{L_2/L_1 - 1} + \frac{1}{k_f L_1}(1 + L_1/L_2)\right]. \quad (29)$$

When L_2/L_1 is large, the bracketed expression reduces to $[1 + \log(k_f L_1) + 1/k_f L_1]$, whence the amount of deceleration increases monotonically as L_1 is decreased. Since the bracketed expression is essentially of order unity except when $k_f L_1$ is exceedingly large, the upstream velocity deficit in this case is essentially proportional to the upwind slope measured relative to f/N.

Finally, in order to illustrate the general dependence of the upstream deceleration on Ro and $\bar{h}_m$, we have computed $u'_{\min}/U$ for the family of Gaussian mountains $h(x) = h_m \exp(-x^2/L^2)$. In Fig. 4 we show contours of constant $u'_{\min}/U$ in the (Ro, $\bar{h}_m$) plane, where Ro $= U/fL$. As predicted by the asymptotics, the amount of blocking is independent of Ro at large Ro; for small Ro, the Coriolis force inhibits the deceleration and, as Ro is decreased, proportionately higher mountains are needed to obtain the same amount of blocking. Of course, the results with $u'_{\min}/U$ of order unity are outside the range of validity of linear theory. Nevertheless, Fig. 4 defines the region of parameter space in which the influence of the mountain is strong.

5. Discussions and applications

In this section we will make use of our results to explore the errors introduced by the use of smoothed terrain. We will be especially concerned with the effect of smoothing on the extent to which a mountain acts as a barrier to the oncoming flow. In some cases we will also be able to suggest strategies for reducing this error. We will also show that preserving the barrier effect introduces other errors, which may or may not be significant.

Our basic result is that, with Ro $= U/(fL)$ and $\bar{h}_m = Nh_m/U$, the relative deceleration upstream of the mountain is $O(\bar{h}_m)$ for large Ro and $O(\mathrm{Ro}\bar{h}_m)$ for small Ro. The numerical results show that if L is characteristic of the half-width of a roughly symmetric mountain, the transition occurs near Ro = 1. Since $\mathrm{Ro}\bar{h}_m = (N/f)(h_m/L)$, the result may be paraphrased by the statement that, for broad mountains it is the slope that counts in determining the barrier effect, while for narrow mountains it is the maximum mountain height that counts. "Broad" in this context means broad compared to U/f.

When a mountain is smoothed in order to permit its representation in a model with finite resolution, its width is increased and its height is decreased, approximately conserving the cross-sectional area of the mountain. This reduces the upstream deceleration by

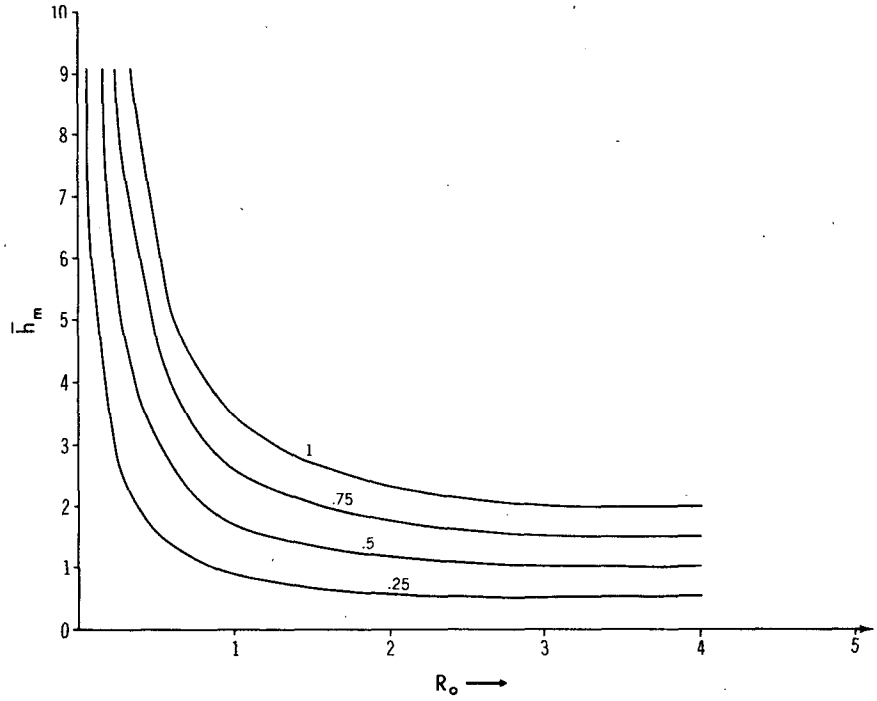

FIG. 4. Contours of constant deceleration (normalized by upstream velocity U) in the (Ro, $\bar{h}_m$) plane. Results shown are for a Gaussian mountain profile of half-width L, and Ro $= U/fL$. As before, $\bar{h}_m = Nh_m/U$.

decreasing both Ro and $\bar{h}_m$. The consequences of this distortion depend on the true values of Ro and $\bar{h}_m$. If the true Ro and $\bar{h}_m$ are in a range where the deceleration is small to begin with, reducing them further is probably of little importance. Suppose the actual deceleration is appreciable, though. If the true Ro is rather greater than unity, then the reduction in deceleration is proportional to the reduction in mountain height. A reasonable correction of the distortion would be to increase the height of the smoothed mountain so that the height of the mountain represented in the numerical model is the same as the height of the original ridge. Thus, *for terrain features with* L < U/f, *the maximum height of the feature in the model topography should be made the same as the maximum height of the actual terrain feature.* We note that this prescription does not distort the vertical scale of the orographic influence, because the depth scale U/N appropriate to the large Ro case is independent of mountain width.

When the true Ro is of order unity or less, the effect of smoothing is even more severe, because the reduction in deceleration is now proportional to both the reduction in Ro and the reduction in $\bar{h}_m$. To preserve the deceleration, the height of the mountain would actually have to be increased in proportion to the increase in width of the smoothed mountain; this is readily seen from the shape of the constant-deceleration contours in Fig. 4. There seems to be no entirely satisfactory resolution of this problem. Increasing the height of the smoothed mountain above the maximum height is undesirable, as it is likely to artificially extend the depth of influence of the mountain. In fact, the depth scale will be artificially enhanced even if the mountain height is not increased, as the depth scale in the regime Ro < O(1) is fL/N. A reasonable compromise would be to preserve the maximum height for larger-scale terrain features as well as for the smaller-scale features. This, at least, represents an improvement over smoothing. Special treatment of broad terrain features would in any event be problematic, as the definition of "broad" depends on the mean wind, which varies considerably with time.

It is instructive to consider some numbers appropriate to the Alps and to the Rocky Mountains. For the Alps, we take half-width $L = 50$ km and typical height $h_m = 2$ km. With $U = 10$ m s^{-1} and $N = 10^{-2}$ s^{-1}, we find Ro = 2 and $\bar{h}_m = 2$. In this range, the Alps are an effective barrier. From either Fig. 3 (representing the Alps as a symmetric triangle of width 100 km) or Fig. 4 (representing the Alps as a Gaussian), it is found that linear theory predicts that the oncoming flow is decelerated essentially to zero at the ground. If the width of the mountain were doubled as a result of smoothing, Ro would fall to 1 and the associated reduction in height would reduce $\bar{h}_m$ to 1. Since the original mountain was in the large Ro regime, Figs. 3 or 4 predict a reduction in deceleration by a factor of 2. If the maximum height had been preserved at 2 km, the deceleration would hardly have decreased at all. Significantly, in the numerical simulations of Bleck (1977) and of Tibaldi and Buzzi (1982) the height of the Alps in the enhanced orography (which led to successful simulations) was 2 km or greater, whereas the height in the smoothed orography was about 1 km or less. We speculate that if the resolution of a model were made great enough to preserve the 2 km height and order-unity Rossby number, no orographic enhancement would be needed. This would occur at a grid spacing of somewhat less than 50 km.

Of course, the appropriate U will vary with the meteorological situation under consideration. If U were increased to 20 m s^{-1}, Ro would increase to 4, putting the mountain well within the large Ro regime. In addition, h_m would decrease to 1, so that the deceleration would decrease to 50% of the oncoming flow. Preserving the maximum height during smoothing would still preserve the deceleration, although, given the lesser deceleration, it might be less important than when $U = 10$ m s^{-1}. Next, suppose $U = 5$ m s^{-1}. Then Ro falls to 1, which implies that smoothing of the mountain moves it into the small Ro regime, whence we conclude that preserving maximum height would no longer be sufficient to preserve the barrier effect. However, with $U = 5$ m s^{-1}, $\bar{h}_m$ increases to 4, implying that the negative perturbation windspeeds on the upwind slope are about twice the basic windspeed U. Therefore, it is likely that nonlinear effects are essential to the understanding of the flow in this parameter range.

The Rocky Mountains have a somewhat greater variety of terrain features. The broad massif extending from the California coast to Denver may be considered to be 2000 km wide and 3 km high. With $U = 10$ m s^{-1} and $N = 10^{-2}$ s^{-1}, this yields Ro = 0.1 (based on half-width) and $\bar{h}_m = 3$. This is well within the small Ro regime, and the indicated decelerations are on the order of 20%. The overall profile of the Rockies is therefore in a rather linear regime, and would not justify any enhancement. However, there are numerous small-scale features of dimensions similar to the Alps embedded in the Rockies, and these will not be adequately resolved in most numerical models. For example, the Sierra Nevada rises from sea level in the San Joaquin Valley to over 2 km in a distance of only 100 km. If the Sierra Nevada were treated as a symmetric triangle, the deceleration would be similar to that occurring upstream of the Alps. In reality, the deceleration will be even greater, since the downwind side of the Sierra Nevada does not come back down to sea level. Preserving the maximum terrain height is necessary in order to retain this deceleration. Even then, the deceleration would be somewhat reduced by extending the upwind slope over a greater distance, since the local Ro will decrease. The barrier effect of

the Sierra Nevada and similar mountains on the west coast of North America is likely to be particularly important, because these are the first mountains encountered by air approaching from the Pacific. It is noteworthy that in smoothed terrain on a 2.5° mesh, the terrain near the California coast rises smoothly from sea level to 1.5 km over a distance of 350 km, whereas the "envelope orography" rises from sea level to 2 km over 210 km (Wallace *et al.*, 1983, Fig. 13).

It must be admitted that smoothing distorts terrain shape as well as scale. A small feature with a steep upwind face will be made more symmetrical by smoothing. As is evident from Fig. 3 and its associated discussion, this would appreciably reduce the deceleration even if the maximum terrain height were preserved. There is no remedy for this problem short of the undesirable expedient of increasing the terrain height above the maximum height of the actual mountain. Preserving maximum height at least reduces the error.

We have seen that preserving the maximum height of a terrain feature as it is broadened improves the retention of the barrier effect in every case, as compared with ordinary smoothing. By increasing the cross-sectional area of the mountain, though, this scheme may lead to undesirable distortions of flow patterns far from the mountain. Consider, for example, the displacement of fluid particles in y occurring far upstream of the mountain. The displacement, which we shall call δy, is defined by

$$U\partial_x(\delta y) = v'. \tag{30}$$

Integrating (30) between two upstream points x_1 and x_2 using the far-upstream form of v' given in (12) yields

$$\delta y = \left(\frac{NA}{\pi U}\right) \ln\left(\frac{x_1}{x_2}\right), \tag{31}$$

where A is the cross-sectional area of the mountain, $\int h(x)dx$. Broadening the mountain while keeping its height fixed increases A and thus exaggerates the deflection occurring between any two far-upstream points.

To determine the importance of this effect, we must estimate the maximum displacement occurring far upstream of the mountain. The area scaling exhibited by (12) and hence (31) is valid only for points far upstream compared to the mountain width L; since it is qualitatively valid at an upstream distance comparable to L, the maximum deflection may be estimated by taking $x_2 = -L$. Even so, the displacement diverges logarithmically as x_1 is removed to $-\infty$. This is an artifact of two-dimensionality; if three-dimensional effects were included, v' would begin to fall off faster than (12) indicates when x_1 approaches the y-scale L_y of the mountain. We therefore estimate the far-upstream deflection around a three-dimensional mountain by taking $x_1 = -L_y$. Assuming further a triangular mountain with half-width L and height h_m, (31) becomes

$$\delta y = \left[\frac{1}{\pi}\left(\frac{Nh_m}{U}\right) \ln\left(\frac{L_y}{L}\right)\right] L. \tag{32}$$

Even with $(L_y/L) = 10$ and $Nh_m/U = 2$, the bracketed quantity multiplying L in (32) is less than 1.5. We conclude that far-upstream effects are unlikely to result in appreciable deflections around ridgelike obstacles. By contrast, arbitrarily large deflections can occur near an obstacle, where the oncoming flow is decelerated almost to rest. It thus seems likely that preserving the near-mountain effects is more important than preserving the area-dependent far-upstream effect, insofar as it is desirable to retain the deflection around the mountain.

We note that some caution must be attached to the results on the far-upstream part of the deflection found in Smith (1982). In an attempt to deal with the nonuniform validity of the large Ro expansion, Smith introduced a modified expansion procedure in which certain inertial terms were retained at lowest order. However, the modified expansion incorrectly predicts the far-upstream velocity field. For example, in the two-dimensional case, Smith's Eq. (13) implies that v is proportional to $1/x^2$ as $x \to -\infty$ (since, in Smith's notation, p_0 is proportional to u' which in turn is proportional to $1/x$). This is manifestly inconsistent with (7), the problem arising because, in Smith's expansion, v adjusts geostrophically to the *near-field* pressure p_0, whereas the true geostrophic adjustment involves the adjustment of both the mass and wind fields. Thus, Smith's approximation leads to an underestimate of the far-field part of the deflection.

Increasing L with fixed h_m also distorts the amplitude of the lee inertial waves; the net effect may be an increase or a decrease, depending on the width of the original mountain. The consequence of this distortion is difficult to determine, as the lee inertial waves are of uncertain meteorological importance.

6. Conclusions

Through a reexamination of a simple model of rotating stratified flow over topography, we have obtained a number of useful results concerning the extent to which flow slows down and turns aside as it approaches a ridgelike mountain. The main controlling parameters are $\mathrm{Ro} = U/(fL)$ (where U is the far-upstream speed perpendicular to the mountain, f the Coriolis parameter, and L a measure of the mountain width) and $\bar{h}_m = Nh_m/U$ (where N is the Brunt-Väisälä frequency and h_m is the maximum height of the mountain). When Ro is large, the deceleration of the impinging flow relative to U is $O(\bar{h}_m)$, but when Ro is small the relative deceleration is $O(\mathrm{Ro}\bar{h}_m) = O[(N/f)(h_m/L)]$. For roughly symmetric mountains with half-width L, the transition

between the two regimes occurs near Ro = 1. For Ro > 1, the flow is decelerated to rest for $\bar{h}_m > 2$, insofar as one can tell from linear theory. The Alps and the steep western slope of the Rocky Mountains were both found to be in a parameter range in which flow would generally be strongly blocked. If terrain is smoothed to permit its representation in a numerical model, L is increased and maximum height is decreased. This reduces both Ro and h_m, and therefore reduces the extent to which the mountain acts as a barrier to flow. The error is particularly severe when the true Ro of the mountain is of order unity or less. We have shown that a better scheme is to preserve the maximum height of the mountain as it is broadened. This strategy in every case improves the retention of the barrier effect, and is in accordance with what has empirically been found to work best in numerical modeling of cyclogenesis in the lee of the Alps.

When Ro is large, a distinction must be made between the character of flow near to, and far from, the mountain (compared to U/f). Near the mountain, the cross-mountain flow is determined by the nonrotating equations and the along-mountain flow is obtained as an O(1/Ro) correction. Far from the mountain Coriolis effects remain dominant. The flow adjusts to geostrophy far upstream. In the near field, the deceleration decays slowly with distance upstream of the mountain, but the decay is rapid in the far field. Comparison of asymptotic with numerical results has shown that the near-field behavior remains qualitatively valid only within a distance U/f from the mountain crest. The comparison also shows that the combination of near- and far-field asymptotic expansions captures almost all the interesting behavior of the system. This suggests the use of such methods in the analysis of more complicated models.

Finally, it must be admitted that our estimates indicate that most mountains of interest are well into the range in which nonlinear effects are important. When nonlinearity is considered, a number of subtle and fundamentally new phenomena are introduced. These effects will be discussed in a future paper.

REFERENCES

Bleck, R., 1977: Numerical simulation of lee cyclogenesis in the Gulf of Genoa. *Mon. Wea. Rev.*, **105,** 428–445.

Buzzi, A., and S. Tibaldi, 1978: Cyclogenesis in the lee of the Alps: A case study. *Quart. J. Roy. Meteor. Soc.*, **104,** 271–288.

Egger, J., 1972: Numerical experiments on cyclogenesis in the Gulf of Genoa. *Beitr. Phys. Atmos.*, **45,** 320–346.

Mesinger, F., and R. F. Strickler, 1982: Effects of mountains on Genoa cyclogeneses. *J. Meteor. Soc. Japan,* **60,** 326–338.

Miles, J. W., and H. E. Huppert, 1969: Lee waves in a stratified flow. Part 4. Perturbation approximations. *J. Fluid Mech.*, **35,** 497–525.

Queney, P., 1947: Theory of perturbations in stratified currents with application to airflow over mountain barriers. Department of Meteorology, University of Chicago, Misc. Rep. No. 23, 67 pp.

Smith, R. B., 1979: The influence of mountains on the atmosphere. *Advances in Geophysics,* Vol. 21, Academic Press, 87–230.

——, 1982: Synoptic observations and theory of orographically disturbed wind and pressure. *J. Atmos. Sci.*, **39,** 60–70.

Tibaldi, S., and A. Buzzi, 1982: Orographic influences on Mediterranean lee cyclogenesis and European blocking in a global numerical model. European Centre for Medium-Range Weather Forecasting, Tech. Rep., No. 29, Reading, England, 46 pp.

Wallace, J. M., S. Tibaldi and A. J. Simmons, 1983: Reduction of systematic forecast errors in the ECMWF model through the introduction of an envelope orography. *Quart. J. Roy. Meteor. Soc.*, **109,** 683–717.